Rare Met. (2021) 40(8):2197–2205
https://doi.org/10.1007/s12598-020-01423-3

RARE METALS
www.editorialmanager.com/rmet

Microstructure, mechanical properties and fracture behavior of a new WE43 alloy

Gui-Long Jia, Li-Ping Wang, Yi-Cheng Feng*, Er-Jun Guo, Yan-Hong Chen, Chang-Liang Wang

Received: 30 May 2018 / Revised: 16 August 2018 / Accepted: 16 April 2020 / Published online: 3 June 2020

Abstract The microstructures, mechanical properties and fracture behaviors of a new WE43 alloy (Mg–4Y–1.6Nd–2Sm–0.5Zr) were investigated. The microstructure of the as-cast alloy includes a Mg matrix, $Mg_{41}Sm_5$, $Mg_{41}Nd_5$ and $Mg_{24}Y_5$ eutectic phases, as well as β-phase. After an optimal solution treatment, the eutectic phases are almost completely dissolved; only a few spots of blocky Mg–Y compounds remain at grain boundaries. After an aging treatment, a large amount of β′-phases are dispersed and precipitated at the grain interior, which provides good comprehensive mechanical properties of the alloy, particularly in the under-aged state. The tensile strength is up to 290 MPa, the yield strength reaches 209 MPa, and the elongation is slightly improved. Furthermore, the fracture behaviors of the studied alloy in different states significantly differ. In addition, a comparison of mechanical properties of the new WE43, traditional WE43 and other modified WE43 alloys is presented.

Keywords Mg–Y–Nd–Sm–Zr; Microstructure; Mechanical properties; Fracture behavior; Heat treatment

1 Introduction

Magnesium alloys have become indispensable materials for crucial components, such as aircraft engine housings, due to their advantages, such as low densities, high specific strengths and specific stiffnesses, excellent electromagnetic shielding and damping capacity [1–4]. Rare earth (RE) elements can purify magnesium alloy melts, improve casting performance and refine grains; in particular, they can enhance mechanical properties, corrosion resistance and wear resistance of traditional magnesium alloys [5–8]. Owing to these advantageous properties, the research and development of Mg–RE alloys have attracted significant interest [9–12].

Extensive studies have been performed on WE43, one of the most popular Mg–RE alloys. Liu et al. [13] prepared a WE43 alloy by differential pressure casting and studied the elevated-temperature tensile deformation behavior of the alloy. The results showed that the tensile stress decreased with the increase in the temperature; however, the effect of the strain rate on the tensile stress above 300 °C was different from that below 300 °C. Zhou et al. [14] applied equal-channel angular pressing (ECAP) to prepare the WE43 alloy. They reported that the multi-pass ECAP process led to multiple evolution of microstructure in WE43, which affected the variations of mechanical properties. In particular, through ECAP with four passes, the average grain size was reduced to 1.5 μm and the microstructure was more homogenous, which provided desirable strength and ductility of the alloy. Kubásek et al. [15] prepared WE43 by powder metallurgy, with excellent mechanical properties and superior corrosion resistance. Moreover, Liu et al. [16] prepared a new Mg–4Y–3Nd–3Dy–0.5Zr alloy by adding Dy to WE43. The content in vol% of precipitates of this alloy was enhanced due to the Dy addition, which provided an improved tensile strength. Liu et al. [17] prepared a modified WE43, in which Nd was partly replaced with Gd. After an optimal T6 treatment, the tensile and yield strengths of the Mg–4Y–2Nd–1Gd–0.4Zr alloy were 297 and 180 MPa, respectively. The room-temperature fracture behaviors of the alloy under different

G.-L. Jia, L.-P. Wang, Y.-C. Feng*, E.-J. Guo, Y.-H. Chen, C.-L. Wang
School of Materials Science and Engineering, Harbin University of Science and Technology, Harbin 150040, China
e-mail: fyc7806067@163.com

thermal conditions were studied by Fu et al. [18]. Using Sm to replace Nd in WE43, Li et al. [19, 20] designed a Mg–4Y–4Sm–0.5Zr alloy with excellent mechanical properties after a T6 treatment; a extrusion processing of the alloy was then performed; the dynamic recrystallization during the extrusion process provided finer grains, leading to further improvements in the mechanical properties. In the above studies, although all the alloys had excellent mechanical properties, either the preparation technology was particularly complex or the RE content was too high, which not only increased the production cost, but also hindered the applications of the alloys. Therefore, it is of significance to develop a new low-cost high-strength WE43 alloy [21].

Sm and Nd are Ce-group light RE elements. The maximum solid solubility of Sm (5.8 wt%) is higher than that of Nd (3.6 wt%) [22]; in addition, Sm is cheaper. Therefore, it is of interest to design a new WE43 alloy (Mg–4Y–1.6Nd–2Sm–0.5Zr) using Sm partly replacing Nd, whose mechanical properties should be better than those of WE43. This design conforms to the current concept of pluralistic development of Mg–RE alloys.

The microstructures, mechanical properties and fracture behaviors of the Mg–Y–Nd–Sm–Zr alloy obtained with different heat treatments were investigated, and an optimal heat treatment process was established. In addition, the WE43 alloy was prepared under the same conditions for comparison. A comparison of mechanical properties of the Mg–Y–Nd–Sm–Zr, traditional WE43 and other modified WE43 alloys was presented.

2 Experimental

The raw materials used in this study were pure Mg, Mg–30%Zr and Mg–30%RE master alloys. The proportion of elements was calculated using the burning loss rate. All the raw materials and tools were preheated at 200 °C. Melting of materials was performed in a pit-type resistance furnace; the melting temperature was 780 °C. In addition, protection gas consisting of SF_6 (1 vol%) and CO_2 (99 vol%) was introduced in the melting process. After the raw materials were completely melted, stirring of the melt for 3 min followed by standing for 30 min was necessary to ensure complete dissolution of all alloying elements; the melt was then cast into a steel permanent mold at a pouring temperature of 760 °C. The chemical compositions of the alloys were measured by inductively coupled plasma-atomic emission spectrometry (ICP-AES, iCAP6300 ICP), and the results are presented in Table 1.

Thermal analyses were performed by differential scanning calorimetry (DSC, Netzsch STA 449F3); the alloys were heated from room temperature to 700 °C, high-purity argon was used as the protection gas, and the heating rate was 10 °C·min^{-1}. The solution treatments were performed in a box-type resistance furnace at 525 °C for 6, 8, 10 and 12 h, followed by quenching in hot water. Aging treatment was performed isothermally at 200 °C for different time periods, followed by cooling in air.

Table 1 Chemical compositions of Mg–Y–Nd–Sm–Zr and WE43 alloys (wt%)

Alloys	Y	Nd	Sm	Zr	Mg
Mg–Y–Nd–Sm–Zr	4.02	1.59	2.03	0.52	Bal
WE43	3.96	3.21	0	0.46	Bal

The microstructures and local chemical compositions of the alloys were analyzed using an optical microscope (OM, Olympus GX71) and a scanning electron microscope (SEM, FEI Sirion 2000) equipped with an X-ray energy dispersive spectrometer (EDS). Phase analyses were performed by an X-ray diffractometer (XRD, X′Pert Pro) with Cu Kα radiation at 40 kV. The precipitates were observed by a transmission electron microscope (TEM, JEM-2100). TEM specimens were mechanically ground to ~ 40 μm, followed by ion milling at an ion-gun energy of ~ 3.6 kV and milling angle of ~ 4°.

Aging responses of the alloys were characterized by age-hardening curves. The hardness was measured by a Vickers hardness meter with a load of 3 N. Room-temperature tensile properties were investigated using a CSS44300 machine for a specimen with a gauge length of 18 mm, width of 5 mm and thickness of 2 mm. The fracture morphologies were observed by SEM.

3 Results and discussion

3.1 Microstructure

OM and SEM images of the as-cast Mg–Y–Nd–Sm–Zr and WE43 alloys are shown in Fig. 1. The microstructures of the as-cast alloys include an equiaxed α-Mg matrix and eutectic phases. Most of the eutectic phases are lamellar and tend to cluster at grain boundaries, and only a small amount of eutectic phase particles are distributed at the grain interior. The average grain size of the Mg–Y–Nd–Sm–Zr alloy is significantly smaller than that of the WE43 alloy.

In order to identify constituents of eutectic phases in the as-cast alloys, XRD was performed; the obtained patterns are shown in Fig. 2. According to XRD patterns and related references, the eutectic phases in the as-cast Mg–Y–Nd–Sm–Zr and WE43 alloys contain $Mg_{24}Y_5$ and $Mg_{41}Nd_5$; in

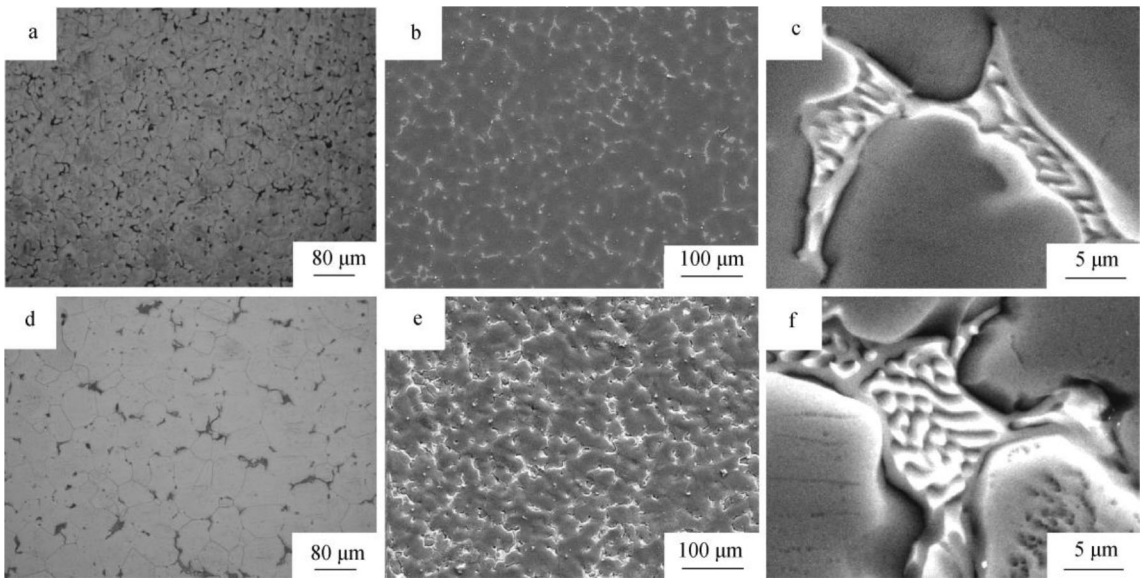

Fig. 1 OM and SEM images of as-cast Mg–Y–Nd–Sm–Zr and WE43 alloys: **a–c** as-cast Mg–Y–Nd–Sm–Zr alloy and **d–f** as-cast WE43 alloy

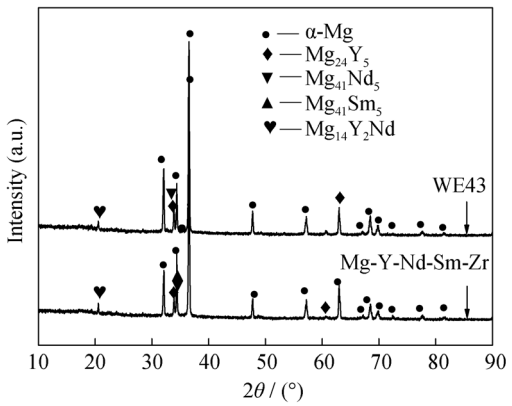

Fig. 2 XRD patterns of as-cast Mg–Y–Nd–Sm–Zr and WE43 alloys

addition, $Mg_{41}Sm_5$ is observed in the former alloy. Furthermore, in addition to the above eutectic phases, β-phase is also observed in the two alloys [23, 24].

In order to provide a basis for the choice of the solution temperature and study the formation temperatures of the eutectic phases, thermal analyses were performed. DSC results of the as-cast alloys are shown in Fig. 3. Three endothermic peaks appear in each DSC curve at 527 and 530 °C, 550 and 544 °C, and 640 and 644 °C successively, which may correspond to the melting temperatures of Mg–Y, Mg–Nd or Mg–Sm phases, and the alloy [25, 26].

SEM images of the Mg–Y–Nd–Sm–Zr and WE43 alloys after solution heat treatments are shown in Fig. 4. It indicates that the larger solution time provided a better solution effect; however, the average grain size becomes abnormally large. There are still large amounts of eutectic phases remaining at grain boundaries after the solution treatment for 6 h, as shown in Fig. 4a. When the solution time is 8 h, the eutectic phases almost dissolve into the Mg matrix and the grains are fine with relatively uniform sizes; however, RE phase spots remain at grain boundaries, as shown in Fig. 4b. With the increase in length, although the solution effect is better, the grain size increases, as shown in Fig. 4c, d. Therefore, it can be deduced that the solution process of the Mg–Y–Nd–Sm–Zr alloy is optimal at 525 °C, performed for 8 h. For comparison, the WE43 alloy is treated with the same solution process. The variation tendency of the microstructures is similar to that of the Mg–Y–Nd–Sm–Zr alloy; however, the solution process of the WE43 alloy is optimal at 525 °C, performed for 10 h, as shown in Fig. 4e–h.

SEM images and EDS spectra of residual RE phases in the solution-treated Mg–Y–Nd–Sm–Zr and WE43 alloys are presented in Fig. 5. The residual RE phases are mostly blocky, approximately cubes, which mainly contain an amount of Y and small amounts of Nd and Sm; therefore, these blocky phases may be insoluble Mg–Y compounds. Furthermore, a few granular phases are observed, containing Y, Nd and Sm, while RE content is not high, suggesting that these granular phases may be undissolved eutectic phases [27, 28].

TEM images and corresponding selected area electron diffraction (SAED) patterns of precipitates at the grain interior of the Mg–Y–Nd–Sm–Zr alloy under different aging states are shown in Fig. 6. TEM images show that after aging at 200 °C for 16 h, a mass of very fine dispersed precipitates are formed at grain interior (Fig. 6a); with the increase in aging time, the precipitates coarsen and their amount decreases, as shown in Fig. 6b, c.

TEM images of precipitates at grain boundaries of Mg–Y–Nd–Sm–Zr alloy under different aging states are shown

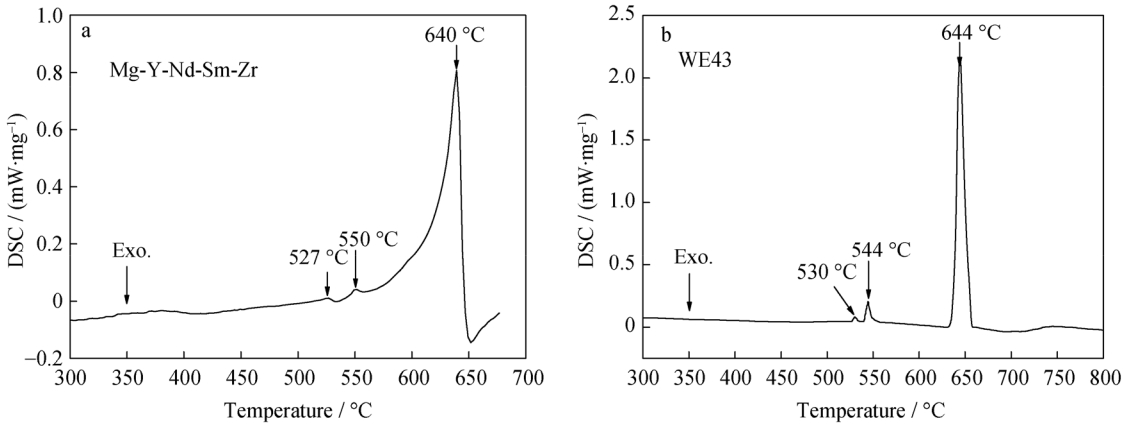

Fig. 3 DSC results of **a** as-cast Mg–Y–Nd–Sm–Zr and **b** WE43 alloys

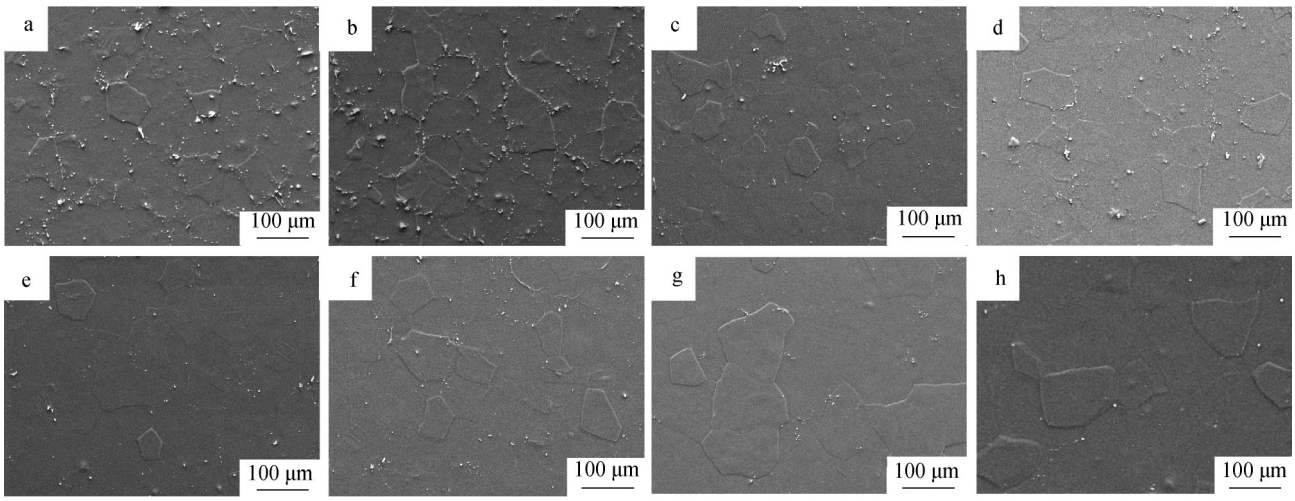

Fig. 4 SEM images of **a–d** Mg–Y–Nd–Sm–Zr and **e–f** WE43 alloys after solution-treated at 525 °C for different times: **a**, **e** 6 h; **b**, **f** 8 h; **c**, **g** 10 h; and **d**, **h** 12 h

in Fig. 7. The size of the precipitates at grain boundaries is significantly larger than that at grain interior. When the aging time is 16 h, the precipitates at grain boundaries have the smallest size, but their number is the largest. With the increase in aging time, the amount of precipitates gradually decreases, while the precipitate size becomes large, as shown in Fig. 7b; the precipitates then substantially coalesce, forming larger-scale precipitates when the aging time increases to 140 h, as shown in Fig. 7c.

3.2 Mechanical properties

Hardness measurements of Mg–Y–Nd–Sm–Zr and WE43 alloys during aging are presented in Fig. 8. The age-hardening curve of Mg–Y–Nd–Sm–Zr alloy shows one-stage aging characteristics, the hardness slowly increases at the initial aging stage, then rapidly increases and reaches the peak-aged stage, followed by a gradual decrease, and finally, the over-aged state is reached. The age-hardening curve of WE43 alloy shows similar aging characteristics to that of Mg–Y–Nd–Sm–Zr alloy; however, the peak hardness is lower and the time required to reach the peak-aged stage is shorter.

Tensile properties of as-cast Mg–Y–Nd–Sm–Zr and WE43 alloys are shown in Fig. 9a. The results show that the mechanical properties of as-cast Mg–Y–Nd–Sm–Zr alloy are better than those of WE43 alloy. The ultimate tensile strength (UTS), yield strength (YS) and elongation (EL) of the as-cast Mg–Y–Nd–Sm–Zr are 200 MPa, 120 MPa and 5%, respectively. Tensile properties of the solution-treated Mg–Y–Nd–Sm–Zr and WE43 alloys are shown in Fig. 9b. The mechanical properties of the solution-treated alloys are slightly improved, but the improvement is not significantly. Moreover, the solution-treated Mg–Y–Nd–Sm–Zr alloy has better mechanical properties. Figure 9c shows tensile properties of the Mg–Y–Nd–Sm–Zr and WE43 alloys under different aging states. In general, with the increase in aging time, the

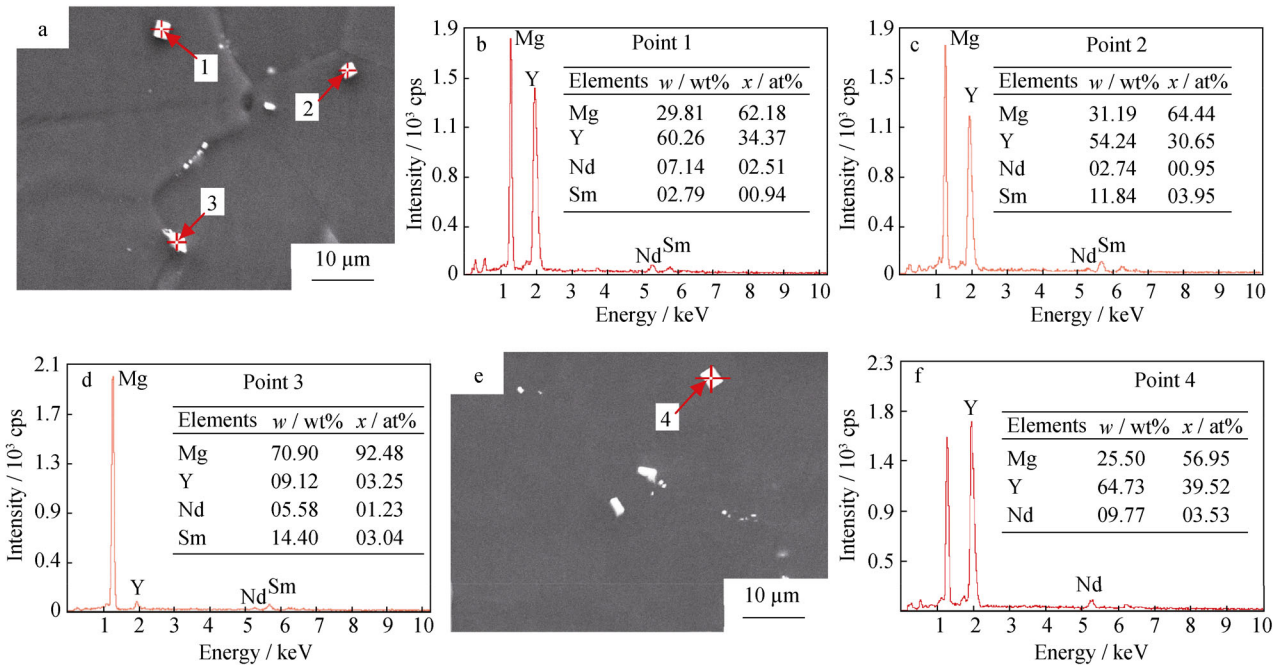

Fig. 5 SEM images and EDS spectra of residual RE phases in solution-treated **a-d** Mg–Y–Nd–Sm–Zr alloy and **e**, **f** WE43 alloy

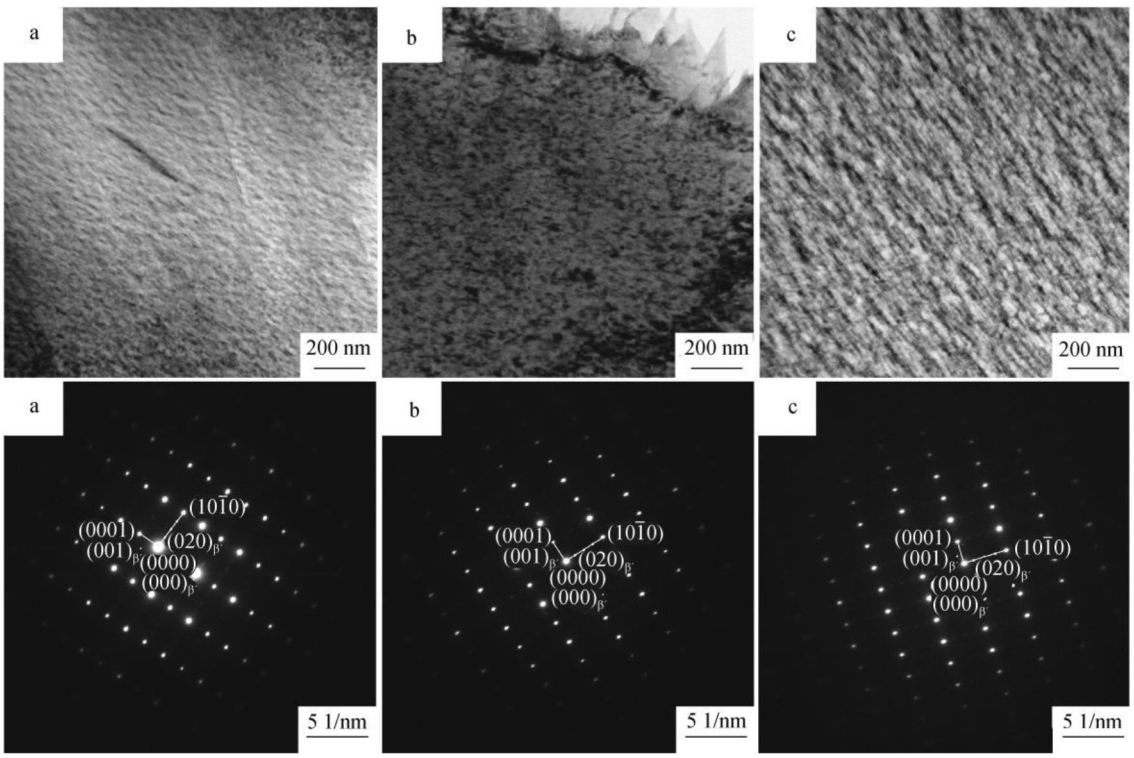

Fig. 6 TEM images and corresponding SAED patterns of precipitates and Mg matrix in Mg–Y–Nd–Sm–Zr alloy under different aging states: **a** under-aged, **b** peak-aged and **c** over-aged beam direction of $[010]_a$

mechanical properties of the alloys at the under-, peak- and over-aged states gradually worsen. Further, the Mg–Y–Nd–Sm–Zr alloy has better mechanical properties under the different aging states than WE43 alloy, particularly at the under-aged state; a maximum UTS of 290 MPa, YS of 209 MPa and EL of 5.7% are obtained. Tensile properties of Mg–Y–Nd–Sm–Zr and WE43 alloys at different states are shown in Fig. 9d. The strength of the as-cast alloy is the

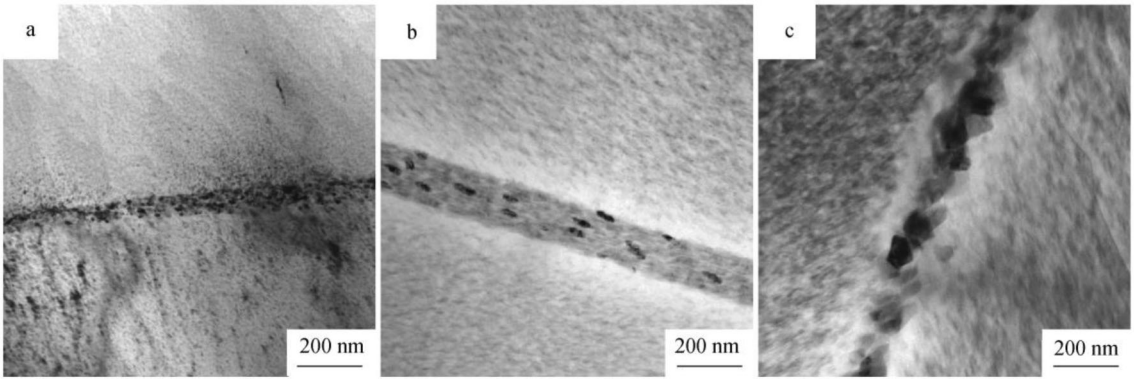

Fig. 7 TEM images of precipitates at grain boundary in Mg–Y–Nd–Sm–Zr alloy under different aging states: **a** under-aged, **b** peak-aged and **c** over-aged

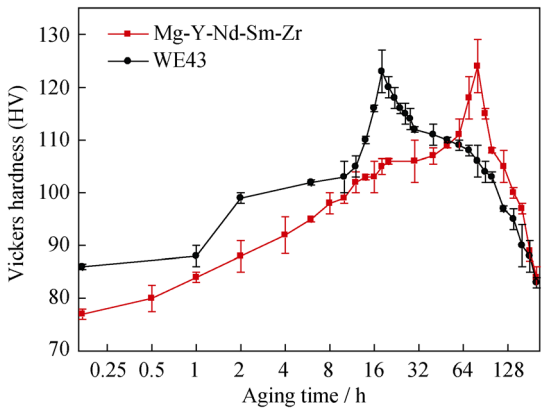

Fig. 8 Age-hardening curves of Mg–Y–Nd–Sm–Zr and WE43 alloys during isothermal aging at 200 °C

lowest, which slightly increases after the solution treatment, while the EL increases significantly. After T6 heat treatment, the alloys exhibit better mechanical properties at the under-aged state. For example, for Mg–Y–Nd–Sm–Zr alloy, compared with as-cast alloy, the UTS of the aged alloy increases by 90 MPa and the EL is also slightly improved. In addition, the maximum strength (290 MPa) of the aged alloy is better than that of the WE43.

Figure 10 shows a comparison of the mechanical properties of the Mg–Y–Nd–Sm–Zr, traditional WE43 and other modified WE43 alloys [15, 17, 23, 29]. The studied alloy at under-aged state exhibits better mechanical properties compared with other modified WE43 alloys in terms of both strength and ductility. Furthermore, the preparation cost of the studied alloy is lower than those of the modified WE43 alloys; therefore, the results obtained for Mg–Y–Nd–Sm–Zr alloy are promising.

3.3 Tensile fracture behavior

Figure 11 shows tensile fractography of Mg–Y–Nd–Sm–Zr and WE43 alloys in different states. The fracture morphology of the as-cast Mg–Y–Nd–Sm–Zr alloy includes a large number of shallow and discontinuous tearing ridges as well as disordered and small cleavage planes. Cleavage steps can be hardly observed on these small cleavage planes; the fractures modes of the as-cast alloy are both intergranular and transgranular fractures. The fracture morphology of the solution-treated alloy is mainly composed of large cleavage planes and developed river patterns. Most of the cleavage planes are connected by tearing ridges. River patterns are also formed by tearing. The fracture mode of the solution-treated alloy is ductile transgranular cleavage fracture. In the fracture morphology of the aged alloy, the cleavage planes are very large, but flatter than those of the solution-treated alloy. The developed river patterns become shallow cleavage steps, while the fracture mode of the aged alloy is brittle transgranular cleavage fracture. The fracture surfaces of the as-cast and aged WE43 alloys are characterized mainly by grain boundaries. Their fracture mode is a typical intergranular fracture. Moreover, the fracture morphology of the solution-treated alloy is similar to that of solution-treated Mg–Y–Nd–Sm–Zr alloy; therefore, the fracture mode of the solution-treated WE43 alloy is also ductile transgranular cleavage fracture [18, 24, 30].

3.4 Discussion

In the thermal analysis of the as-cast Mg–Y–Nd–Sm–Zr alloy, the result of the DSC trace provides a basis for the choice of the solution temperature (slightly lower than the melting temperatures of the eutectic phases). After the solution process at 525 °C for 8 h, the eutectic phases are almost dissolved into the matrix, the grains are fine, and their sizes are relatively uniform. Although there are still a few blocky Mg–Y compounds remaining at the grain boundaries, the solution process for the Mg–Y–Nd–Sm–Zr alloy performed at 525 °C for 8 h is optimal.

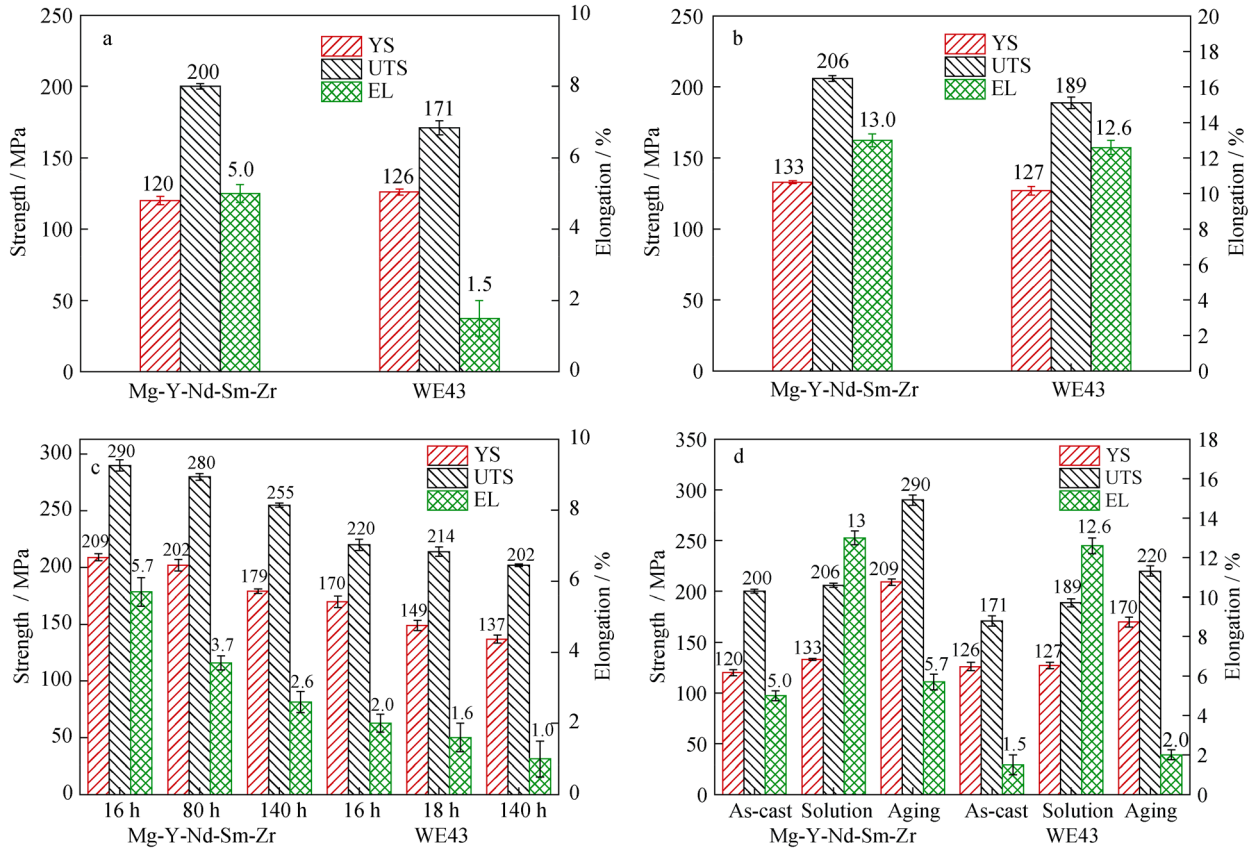

Fig. 9 Tensile properties of **a** as-cast Mg–Y–Nd–Sm–Zr and WE43 alloys, **b** solution-treated Mg–Y–Nd–Sm–Zr (525 °C × 8 h) and WE43 alloys (525 °C × 10 h), **c** Mg–Y–Nd–Sm–Zr and WE43 alloys under different aging states (under-aged: 16 h; peak-aged: 80 h; over-aged: 140 h) and **d** Mg–Y–Nd–Sm–Zr and WE43 alloys in different states (as-cast; solution: 525 °C × 8 h/525 °C × 10 h; aging: 200 °C, 16 h)

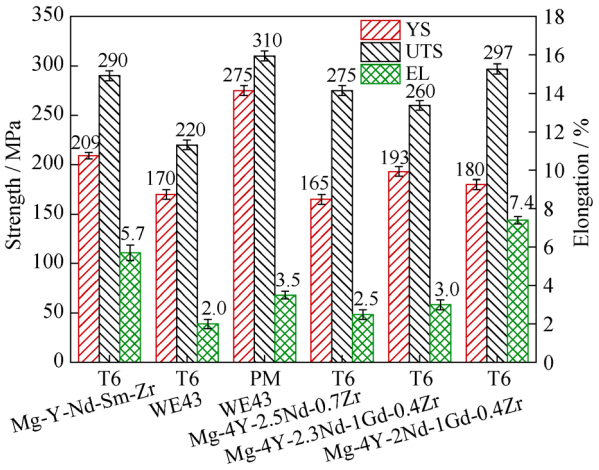

Fig. 10 A comparison of mechanical properties of Mg–Y–Nd–Sm–Zr, traditional WE43 and other modified WE43 alloys (PM being powder metallurgy)

In the studied alloy, the light RE elements Sm and Nd provide a strong precipitation strengthening effect; the one-stage aging characteristic of the age hardening curve is very similar to those of Ce-group light RE elements in magnesium alloys.

In the as-cast alloy, as the eutectic phases segregated at grain boundaries are brittle, stress concentration easily emerges. Upon a tensile force, initial cracks form at eutectic phases and induce fracture, which is the main origin of the poor mechanical properties of the as-cast alloy. After the solution treatment, the eutectic phases are almost dissolved into the Mg matrix and solution strengthening effect is observed, leading to an improvement in strength of the solution-treated alloy compared with the as-cast alloy. The dissolution of eutectic phases and homogenous distribution of alloying elements are the origins of the increase in elongation. After the typical T6 heat treatment, a mass of very fine precipitates are uniformly dispersed at the grain interior. The orientation relationship between the precipitates and Mg matrix, revealed by the SAED pattern, indicates that the precipitates are β′-phases [28, 31, 32]. These β′-phases can effectively block dislocation movement, which leads to an improved strength of the alloy. Therefore, the solution strengthening and precipitation hardening of the alloying elements Y, Nd and Sm are the main strengthening

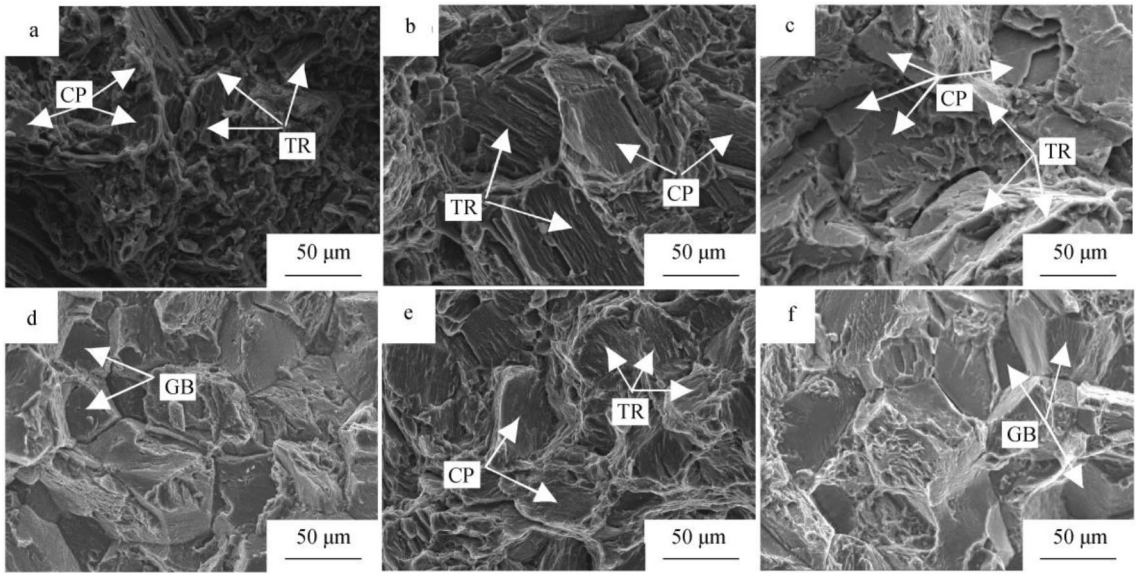

Fig. 11 Tensile fracture SEM images of **a–c** Mg–Y–Nd–Sm–Zr and **d-f** WE43 alloys in different states: **a**, **d** as-cast; **b**, **e** solution-treated; **c**, **f** aged (TR being tearing ridge; CP being cleavage plane; GB being grain boundary)

mechanism of the alloy. Furthermore, blocky Mg–Y compounds that remain at grain boundaries lead to a strong tearing effect on the magnesium matrix; therefore, these compounds negatively affect the mechanical properties of the alloy.

The size and distribution of the precipitates at the grain interior and boundaries affect the mechanical properties of the alloy under different aging states. Although the precipitates at the grain interior under different aging states are β′-phases which can efficiently improve mechanical properties, the β′-phases in the under-aged state are very fine and their distribution is more uniform. In addition, the precipitates at grain boundaries are relatively small, providing the best mechanical properties of the alloy in the under-aged state. With the increase in aging time, β′-phases grow up and coarsen, and the precipitates at grain boundaries form large-scale precipitates, leading to a gradual performance reduction in terms of the mechanical properties in the peak and over-aged states. Therefore, the aging process for Mg–Y–Nd–Sm–Zr alloy is optimal at 200 °C, performed for 16 h.

In the as-cast alloy, initial cracks preferentially form at grain boundaries due to the formation of high stress concentration at the eutectic phases. The cracks then extend along the grain boundaries to form an intergranular fracture, or into the grain to form a transgranular fracture. After the solution treatment, the dissolution of eutectic phases effectively eliminates stress concentration; the strength of the grain boundaries is improved, compared with that of the as-cast alloy. Initial cracks form at grain interior and extend to grain boundaries. Owing to the solution strengthening, cracks are subjected to a larger resistance while expanding through the grains, leading to the formation of a transgranular cleavage fracture. The developed river patterns in the fracture morphology also correspond to the highest elongation of the alloy. After aging treatment, a mass of very fine β′-phases are precipitated at grain interior, and these dispersed β′-phases can block dislocation movement and form a dislocation pileup. Therefore, initial cracks form at grain interior and extend to grain boundaries, leading to the formation of a transgranular cleavage fracture.

4 Conclusion

In this study, the microstructure of the as-cast Mg–Y–Nd–Sm–Zr alloy included Mg matrix, $Mg_{41}Sm_5$, $Mg_{41}Nd_5$ and $Mg_{24}Y_5$ eutectic phase, as well as β-phase. After solution-treated at 525 °C for 8 h, the eutectic phases were almost completely dissolved; only a few blocky Mg–Y compounds remained at grain boundaries. A large amount of β′-phases were dispersed and precipitated at the grain interior in the under-aged state, providing good mechanical properties of the alloy, with a UTS of 290 MPa, YS of 209 MPa and EL of 5.7%, better than those of traditional WE43 and other modified WE43 alloys. The heat treatment of the studied alloy was optimal when the solution process was performed at 525 °C for 8 h, followed by aging at 200 °C for 16 h. The tensile fracture mode of the as-cast alloy was a mixed transgranular and intergranular fracture, while those of the solution-treated and aged alloys were transgranular cleavage fracture.

Acknowledgements This study was financially supported by the Natural Science Foundation of Heilongjiang Province (No. E2018045).

References

[1] Zhang WL, Xiao DH, Li T, Du JD, Ding DY. Microstructure and mechanical properties of two-stage aged Al–Cu–Mg–Ag–Sm alloy. Rare Met. 2019;38(1):42.
[2] Wang Y, Xiong BQ, Li ZH, Huang SH, Wen K, Li XW, Zhang YA. As-cast microstructure of Al–Zn–Mg–Cu–Zr alloy containing trace amount of Sc. Rare Met. 2019;38(4):343.
[3] Zhang M, Deng WL, Yang XN, Wang YK, Hang RQ, Deng KK, Huang XB. In vitro biodegradability of Mg–2Gd–*x*Zn alloys with different Zn contents and solution treatments. Rare Met. 2019;38(7):620.
[4] Deng KK, Shi JY, Wang CJ, Wang XJ, Wu YW, Nie KB, Wu K. Microstructure and strengthening mechanism of bimodal size particle reinforced magnesium matrix composite. Compos A. 2012;43(8):1280.
[5] Qiu X, Yang Q, Guan K, Bu FQ, Cao ZY, Liu YB, Meng J. Microstructures and tensile properties of Mg-Zn-(Gd)-Zr alloys extruded at various temperatures. Rare Met. 2017;36(12):962.
[6] Wang G, Guo CX, Pang SJ. Thermal stability, mechanical properties and corrosion behavior of a Mg-Cu-Ag-Gd metallic glass with Nd addition. Rare Met. 2017;36(3):183.
[7] Jiang HS, Qiao XG, Zheng MY, Wu K, Xu C, Kamado S. The partial substitution of Y with Gd on microstructures and mechanical properties of as-cast and as-extruded Mg-10Zn-6Y-0.5Zr alloy. Mater Charact. 2018;135:96.
[8] Yu HH, Li CZ, Xin YC, Chapuis A, Huang XX, Liu Q. The mechanism for the high dependence of the Hall-Petch slope for twinning/slip on texture in Mg alloys. Acta Mater. 2017;128:313.
[9] Liu H, Ju J, Bai J, Yang XY, Li YH, Jiang JH, Ma AH. Microstructure and mechanical property of Mg-10Gd-2Y-1.5Zn-0.5Zr alloy processed by eight-pass equal-channel angular pressing. Rare Met. 2018. https://doi.org/10.1007/s12598-018-1022-1.
[10] Jung IH, Sanjari M, Kim J, Yue S. Role of RE in the deformation and recrystallization of Mg alloy and a new alloy design concept for Mg-RE alloys. Scripta Mater. 2015;102:1.
[11] Yue XD, Li JR, Wang XG. The microstructure of a single crystal superalloy after different aging heat treatments. Rare Met. 2018;37(3):210.
[12] Tekumalla S, Seetharaman S, Almajid A, Gupta M. Mechanical properties of magnesium-rare earth alloy systems: a review. Metals. 2014;5(1):1.
[13] Liu HH, Ning ZL, Sun HC, Cao FY, Wang H, Zhao XY, Sun JF. Microstructure and elevated-temperature tensile properties of differential pressure sand cast Mg-4Y-3Nd-0.5Zr alloy. China Foundry. 2016;13(1):30.
[14] Zhou L, Liu Y, Zhang J, Kang Z. Microstructure and mechanical properties of equal channel angular pressed Mg-Y-RE-Zr alloy. Mater Sci Technol. 2016;32(10):969.
[15] Kubásek J, Dvorský D, Čavojský M, Vojtěch D, Beronská N, Fousová M. Superior properties of Mg-4Y-3RE-Zr alloy prepared by powder metallurgy. J Mater Sci Technol. 2017;33(7):652.
[16] Liu HH, Ning ZL, Yi JY, Ma Q, Sun HC, Huang YJ, Sun JF. Effect of Dy addition on microstructure and mechanical properties of Mg-4Y-3Nd-0.4Zr alloy. Chin J Nonferrous Met. 2017;27(4):979.
[17] Liu ZJ, Wu GH, Liu WC, Pang S, Ding WJ. Effect of heat treatment on microstructures and mechanical properties of sand-cast Mg-4Y-2Nd-1Gd-0.4Zr magnesium alloy. Chin J Nonferrous Met. 2012;22(7):1540.
[18] Fu PH, Peng LM, Jiang HY, Zhang ZY, Zhai CQ. Fracture behavior and mechanical properties of Mg-4Y-2Nd-1Gd-0.4Zr (wt%) alloy at room temperature. Mater Sci Eng A. 2008;486(1–2):572.
[19] Li DQ, Wang QD, Ding WJ. Effects of samarium on microstructure and mechanical properties of Mg-Y-Sm-Zr alloys during thermo-mechanical treatments. J Mater Sci. 2009;44(12):3049.
[20] Li DQ, Wang QD, Ding WJ, Blandin JJ, SuÉRy M. Influence of extrusion temperature on microstructure and mechanical properties of Mg-4Y-4Sm-0.5Zr alloy. Chin J Nonferrous Met. 2010;20(7):1311.
[21] Wang XJ, Xu DK, Wu RZ, Chen XB, Peng QM, Jin L, Xin YC, Zhang ZQ, Liu Y, Chen XH, Deng KK, Wang HY. What is going on in magnesium alloys? J Mater Sci Technol. 2017;34(2):245.
[22] Liu NY, Zhang ZY, Peng LM, Ding WJ. Microstructure evolution and mechanical properties of Mg-Gd-Sm-Zr alloys. Mater Sci Eng A. 2015;627:223.
[23] Xu L, Liu CM, Wan YC, Wang X, Xiao HC. Effects of heat treatments on microstructures and mechanical properties of Mg-4Y-2.5Nd-0.7Zr alloy. Mater Sci Eng A. 2012;558:1.
[24] Zhang HH, Fan JF, Zhang L, Wu GH, Liu WC, Cui WD, Feng S. Effect of heat treatment on microstructure, mechanical properties and fracture behaviors of sand-cast Mg-4Y-3Nd-1Gd-0.2Zn-0.5Zr alloy. Mater Sci Eng A. 2016;677:411.
[25] Li YJ, Zhang K, Zhang Y, Li XG, Ma ML. Microstructural evolution and mechanical properties of Mg-5Y-5Gd-*x*Nd-0.5Zr magnesium alloys at different states. Rare Met. 2010;29(3):317.
[26] Yin H, Liu ZL, Liu XQ, Fan RY, Liu Y, Li J. Effects of Al addition on the microstructure and mechanical properties of Mg-4Y alloys. Mater Sci Technol. 2017;33(18):2188.
[27] Liu QZ, Ding XF, Liu YP, Wei XJ. Analysis on micro-structure and mechanical properties of Mg-Gd-Y-Nd-Zr alloy and its reinforcement mechanism. J Alloys Comp. 2017;690:961.
[28] Tian Z, Yang Q, Guan K, Meng J, Cao ZY. Microstructure and mechanical properties of a peak-aged Mg-5Y-2.5Nd-1.5Gd-0.5Zr casting alloy. J Alloys Comp. 2018;731:704.
[29] Kang YH, Yan H, Chen RS. Effects of heat treatment on the precipitates and mechanical properties of sand-cast Mg-4Y-2.3Nd-1Gd-0.6Zr magnesium alloy. Mater Sci Eng A. 2015;645:361.
[30] Zhao SC, Guo EJ, Cao GJ, Wang LP, Lun YC, Feng YC. Microstructure and mechanical properties of Mg-Nd-Zn-Zr alloy processed by integrated extrusion and equal channel angular pressing. J Alloys Comp. 2017;705:118.
[31] Li DQ, Wang QD, Ding WJ. Characterization of phases in Mg-4Y-4Sm-0.5Zr alloy processed by heat treatment. Mater Sci Eng A. 2006;428(1–2):295.
[32] Xin RL, Li L, Zeng K, Song B, Liu Q. Structural examination of aging precipitation in a Mg-Y-Nd alloy at different temperatures. Mater Charact. 2011;62(5):535.